Atmospheric Environment 156 (2017) 77–87

Contents lists available at ScienceDirect

Atmospheric Environment

journal homepage: www.elsevier.com/locate/atmosenv

Composition and sources of winter haze in the Bakken oil and gas extraction region

A.R. Evanoski-Cole [a], K.A. Gebhart [b], B.C. Sive [c], Y. Zhou [a], S.L. Capps [d], D.E. Day [e], A.J. Prenni [c], M.I. Schurman [a], A.P. Sullivan [a], Y. Li [a, 1], J.L. Hand [e], B.A. Schichtel [b], J.L. Collett Jr. [a, *]

[a] Department of Atmospheric Science, Colorado State University, 1371 Campus Delivery, Fort Collins, CO 80523, USA
[b] National Park Service, Air Resources Division, Fort Collins, CO, USA
[c] National Park Service, Air Resources Division, Lakewood, CO, USA
[d] Department of Mechanical Engineering, University of Colorado Boulder, Boulder, CO, USA
[e] Cooperative Institute for Research in the Atmosphere (CIRA), Colorado State University, Fort Collins, CO, USA

HIGHLIGHTS

- Measured wintertime aerosol and aerosol precursors in National Parks.
- Discovered regionally elevated $PM_{2.5}$ concentrations in the Bakken region.
- High $PM_{2.5}$ concentrations associated with air mass stagnation or recirculation.
- VOC measurements link elevated $PM_{2.5}$ concentrations to oil and gas activities.

GRAPHICAL ABSTRACT

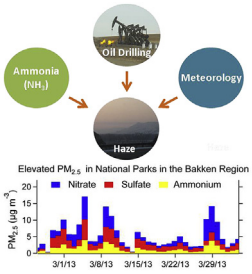

ARTICLE INFO

Article history:
Received 11 August 2016
Received in revised form
6 February 2017
Accepted 8 February 2017
Available online 9 February 2017

Keywords:
Oil and natural gas
Bakken
Aerosol
Particulate matter
Haze

ABSTRACT

In the past decade increased use of hydraulic fracturing and horizontal drilling has dramatically expanded oil and gas production in the Bakken formation region. Long term monitoring sites have indicated an increase in wintertime aerosol nitrate and sulfate in this region from particulate matter ($PM_{2.5}$) measurements collected between 2000 and 2010. No previous intensive air quality field campaign has been conducted in this region to assess impacts from oil and gas development on regional fine particle concentrations. The research presented here investigates wintertime $PM_{2.5}$ concentrations and composition as part of the Bakken Air Quality Study (BAQS). Measurements from BAQS took place over two wintertime sampling periods at multiple sites in the United States portion of the Bakken formation and show regionally elevated episodes of $PM_{2.5}$ during both study periods. Ammonium nitrate was a major contributor to haze episodes. Periods of air stagnation or recirculation were associated with rapid increases in $PM_{2.5}$ concentrations. Volatile organic compound (VOC) signatures suggest that air masses during these episodes were dominated by emissions from the Bakken region itself. Formation rates of alkyl nitrates from alkanes revealed an air mass aging timescale of typically less than a day for periods with elevated $PM_{2.5}$. A thermodynamic inorganic aerosol model (ISORROPIA) was used to investigate gas-particle partitioning and to examine the sensitivity of $PM_{2.5}$ concentrations to aerosol

* Corresponding author. Colorado State University, Department of Atmospheric Science, 200 West Lake Street, 1371 Campus Delivery, Fort Collins, CO 80523-1371, USA.
E-mail address: collett@atmos.colostate.edu (J.L. Collett).
[1] Now at Arizona Department of Environmental Quality, Air Quality Division, Phoenix, AZ, USA.

http://dx.doi.org/10.1016/j.atmosenv.2017.02.019

precursor concentrations. Formation of ammonium nitrate, the dominant component, was most sensitive to ammonia concentrations during winter and to nitric acid concentrations during early spring when ammonia availability increases. The availability of excess ammonia suggests capacity for further ammonium nitrate formation if nitrogen oxide emissions increase in the future and lead to additional secondary formation of nitric acid.

1. Introduction

The Bakken Formation, a subsurface of the Williston Basin, spans an area of 520,000 km^2 over western North Dakota and eastern Montana in the United States (U.S.) and extends into the Canadian provinces of Manitoba and Saskatchewan. This basin has been actively drilled since the 1950s, but production of oil drastically increased since 2006 due to improvements in horizontal drilling and hydraulic fracturing techniques. An estimated 7.38 billion barrels of oil is recoverable in the U.S. portion of the Williston Basin (Gaswirth and Marra, 2015), which includes both the Bakken formation and the underlying Three Forks formation which is often included with the Bakken formation. During the Bakken Air Quality Study (BAQS) period, over one third of the captured natural gas was burned off in flaring (U.S. Energy Information Administration, 2014a) because the region lacked the infrastructure or pipelines to safely store and transport natural gas. More recently North Dakota state regulations have led to the completion of natural gas infrastructure which resulted in sharp reductions in natural gas flaring (U.S. Energy Information Administration, 2016). In parallel to increases in oil production and flaring, other anthropogenic activities associated with the oil and gas industry increased. These include increases in vehicle emissions and generation of road dust (Choi and Roberts, 2015) from diesel truck traffic, greater numbers of diesel engines used during drilling operations, and an increased population needed to support the expanded oil industry. The development of the oil sands in eastern Alberta, Canada is a major source of particulate matter (PM) and aerosol precursors (Liggio et al., 2016; McLinden et al., 2012; Wiklund et al., 2012) which also might impact the Bakken region by long range transport. The effect these anthropogenic sources have on the regional PM has not been previously studied in detail.

Different processes and activities associated with oil and natural gas extraction can emit PM directly or emit gaseous precursors that can later form PM if favorable conditions exist for particle formation. Emissions inventories from the Bakken (Grant et al., 2014a) and several other U.S. natural gas basins (e.g. Bar-Ilan et al., 2008; Grant et al., 2014b) have been developed for unconventional drilling techniques, providing estimates for emissions of methane and other volatile organic compounds (VOCs), nitrogen oxides (NO_x), ozone, other hazardous air pollutants, and PM which are emitted from different sources associated with oil and gas development. However, detailed aerosol composition measurements are lacking in the Bakken region. Inorganic particle formation from the precursor gases ammonia, nitrogen oxides and sulfur dioxide from local or regional sources can create inorganic ammonium nitrate (AN) and ammonium sulfate (AS) particles (Seinfeld and Pandis, 2006). Organic aerosol in the Bakken could originate from both primary emissions and secondary formation from both local sources and long-range transport. For example, VOCs can react with NO_x to form particulate organic nitrate, which has been observed near oil and gas operations in the Uintah Basin in Utah (Lee et al., 2014). Black carbon (BC) can be emitted from diesel trucks and industrial stationary diesel engines (Khalek et al., 2015; U.S. Environmental Protection Agency, 2012) or from flaring (Giwa et al., 2014; Stohl et al., 2013). In the Bakken region, additional local and regional sources of precursor gases and aerosol from coal-fired power plants, agriculture, and increased population and traffic can potentially contribute further to elevated concentrations of PM.

Long term measurements of PM less than 2.5 μm in aerodynamic diameter ($PM_{2.5}$) by the Interagency Monitoring of Protected Visual Environments (IMPROVE) program have shown increases in $PM_{2.5}$ sulfate and nitrate in the Bakken region in the winter (Hand et al., 2012), contrasting decreasing trends across much of the U.S. The trends presented by Hand et al. focused on 2000–2010 while oil production did not rapidly accelerate until 2007 when the Parshall Field was discovered (U.S. Energy Information Administration, 2014b) as shown in Fig. S1. To better understand wintertime aerosol concentrations and composition in the Bakken region and how they are changing with regional changes in oil and gas production, BAQS was conducted over two wintertime periods in 2013 and 2014.

An overview of BAQS detailing the sources and characterization of primary emissions is provided in Prenni et al. (2016). Here we focus on the development and characteristics of winter fine particle haze episodes. Wintertime haze episodes are investigated using aerosol scattering and meteorological variables. Analysis of back trajectories gives insight into the transport patterns associated with observed $PM_{2.5}$ episodes. VOC measurements will be examined to characterize timescales of haze formation and to assess the impact from oil and natural gas operations. A detailed analysis of the aerosol composition, including both inorganic and carbonaceous components, will be discussed. This will include the general characteristics of the $PM_{2.5}$ and contributions of each species to total $PM_{2.5}$ mass. Finally, gas to particle partitioning of the inorganic species will be explored using a thermodynamic aerosol model. The model is also used to analyze sensitivities of aerosol formation to concentrations of inorganic precursor gases.

2. Methods

2.1. Field study overview

An initial pilot study (BAQS I) was conducted between February 15 and April 6, 2013 and a second study (BAQS II) was conducted the following winter between November 23, 2013 and March 28, 2014. Fig. 1 shows four BAQS sampling site locations used in this analysis along with the active oil and gas wells in 2013 in the Bakken formation. Knife River Indian Villages National Historic Site (KNRI) is located to the east of the main area of drilling, but close to several major coal-fired power plants. Medicine Lake National Wildlife Refuge (MELA) is located to the west of the main area of drilling in Montana. Fort Union Trading Post National Historic Site (FOUS) and the North Unit of Theodore Roosevelt National Park (THRO-N) are both located within the most active area of drilling. At KNRI, 48-h time integrated aerosol ionic composition and inorganic gas measurements were obtained during BAQS I. MELA, FOUS and THRO-N had instrumentation to measure aerosol ionic composition

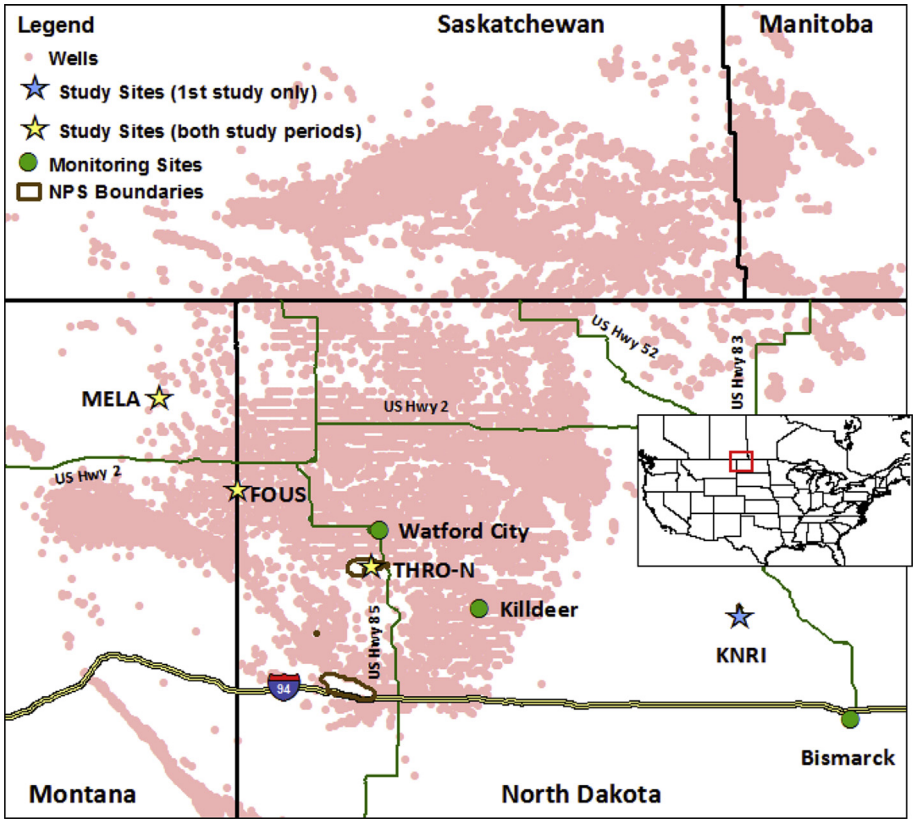

Fig. 1. A map of eastern Montana and western North Dakota in the United States and southern Manitoba and Saskatchewan in Canada shows the locations of sampling sites during BAQS and active oil wells. See text for site names. All study sites were used in the first study from February–April 2013 (yellow and blue stars). The second study from November 2013–March 2014 focused on MELA, FOUS and THRO-N (yellow stars). National park lands are outlined in brown. Active gas and oil wells through the year 2014 are labeled with pink circles. Meteorological data were taken from three additional monitoring sites (green circles). (For interpretation of the references to colour in this figure legend, the reader is referred to the web version of this article.)

and inorganic precursor gases at daily, 48-h or weekly time resolution during both studies. In addition, THRO-N featured a comprehensive suite of instrumentation during BAQS II to measure VOCs and high-resolution aerosol composition and inorganic precursor gas concentrations. All measurements presented in this study are summarized in Tables S1 and S2. For a complete list and schedule of measurements from both field studies, refer to Prenni et al. (2016).

2.2. Instrumentation and analysis methods

A University Research Glassware (URG) Corporation annular denuder/filter-pack sampler was used to capture both inorganic gases and aerosol (Benedict et al., 2013; Lee et al., 2008; Yu et al., 2006, 2005). The sampler first draws ambient air through a Teflon-coated $PM_{2.5}$ cyclone to remove particles with aerodynamic diameters greater than 2.5 μm. Next, a sodium bicarbonate coated glass annular denuder captures nitric acid (HNO_3) and sulfur dioxide (SO_2) and a phosphorous acid coated denuder captures ammonia (NH_3). A filter pack with a 37 mm diameter nylon filter (Pall Nylasorb) captures $PM_{2.5}$. Finally, an additional phosphorous acid coated denuder was placed after the filter to capture any NH_3 that was volatilized from AN initially captured on the filters. Any volatilized HNO_3 from collected particulate AN is retained on the nylon filter (Yu et al., 2005). Samples were collected at a nominal flow rate of 10 L min^{-1}. Total sample air volume was monitored with a dry gas meter and corrected for the pressure drop through the sample train. Denuder and filter samples were extracted in 18.2 MΩ deionized water and analyzed using ion chromatography to quantify gaseous NH_3, HNO_3, and SO_2 and $PM_{2.5}$ sodium (Na^+), ammonium (NH_4^+), potassium (K^+), magnesium (Mg^{2+}), calcium (Ca^{2+}), chloride (Cl^-), nitrite (NO_2^-), nitrate (NO_3^-) and sulfate (SO_4^{2-}). Daily calibrations using prepared anion and cation standards were performed. Sample blanks, replicates and standards prepared from Dionex NIST-traceable anion and cation standards were analyzed periodically. URG measurement precision is 5–9% relative standard deviation for $PM_{2.5}$ NO_3^-, SO_4^{2-} and NH_4^+ and HNO_3, SO_2 and NH_3. The precision for the remaining species is 8–22% relative standard deviation (Lee et al., 2008).

A MARGA, or Monitor for AeRosol and Gases in ambient Air (Makkonen et al., 2014; Rumsey et al., 2014) made hourly measurements at THRO-N during the second study of the same inorganic precursor gases and $PM_{2.5}$ inorganic species as the URG measurement as well as nitrous acid (HNO_2). The MARGA (Metrohm/Applikon) uses a wet-rotating glass denuder to capture inorganic gases (Trebs et al., 2004; Wyers et al., 1993), a steam jet aerosol collector (Khlystov et al., 1995; Slanina et al., 2001) to collect water-soluble inorganic aerosol components, and ion chromatography for analysis. For the inlet, a Teflon coated $PM_{2.5}$ cyclone was used with polyethylene tubing kept as short as possible (1.7 m) to minimize losses of gases. A blank sample was run weekly and external standards were used to verify the internal MARGA calibration. A previous comprehensive study investigated the MARGA accuracy and precision, compared to URG measurements, which is detailed in Rumsey et al. (2014). Measurement precision for $PM_{2.5}$ NO_3^-, SO_4^{2-} and NH_4^+ and HNO_3, SO_2 and NH_3 is 3–23%

median average relative percent difference. Additionally, MARGA measurements were verified with URG measurements and linear regression analysis was used to correct MARGA concentrations of NH_4^+, Mg^{2+}, and Ca^{2+} as described in the supplement and Fig. S2.

A Magee Scientific 7-wavelength dual-spot aethalometer (Drinovec et al., 2015; Hansen et al., 1984) measured black carbon in $PM_{2.5}$ (BC) at THRO-N during both studies. Teflon filters were collected during BAQS I and II and quartz filters were collected during BAQS II using the IMPROVE modules A and C (Hand, 2011), respectively, at THRO-N. Total $PM_{2.5}$ mass was measured gravimetrically using the Teflon filters (Malm et al., 2011). Quartz filters were analyzed by thermal optical reflectance for organic and elemental carbon using the IMPROVE method (Chow et al., 2007; Malm, 2004). A tapered element oscillating microbalance (TEOM, Thermo Scientific 1405-DF) also measured total $PM_{2.5}$ mass at THRO-N during BAQS II. An Aerodyne High-Resolution Time-of-Flight Aerosol Mass Spectrometer (AMS) (Decarlo et al., 2006; Drewnick et al., 2005; Jayne et al., 2000) measured non-refractory PM_1 (PM less than ~1 μm in aerodynamic diameter) providing quantitative measurements of inorganic species Cl^-, NO_3^-, SO_4^{2-} and NH_4^+ along with total organic mass at THRO-N during BAQS II. The AMS concentrations presented here are 5-min averages of samples collected using the high sensitivity V-mode and processed according to the procedure described in Schurman et al. (2015a,b). Nephelometers (Heintzenberg et al., 2006; Müller et al., 2009) were deployed to directly measure light extinction due to scattering by particles (b_{sp}). An NGN-2 Optec nephelometer was operated in an open-air configuration with a wavelength of 550 nm at FOUS. Radiance Research M903 (THRO-N) and Ecotech M9003 (KNRI for BAQS I and MELA for BAQS II) nephelometers used a $PM_{2.5}$ inlet and measured scattering at 530 nm and 520 nm, respectively. Each nephelometer was calibrated weekly with span gas and zero air. The NGN-2 and Ecotech instruments were operated at ambient conditions. The Radiance Research instrument was housed indoors (~15 °C) throughout both studies, so the samples experienced significant warming and associated reductions in humidity for the measurements. All aerosol instrument inlets were unheated.

Whole air grab samples for VOC analysis were collected during BAQS II in clean and evacuated 2 L stainless steel canisters twice a day at THRO-N, four times a week at FOUS and once a week at MELA. A suite of VOCs were analyzed on a custom 5-channel gas chromatography system utilizing three flame ionization detectors, an electron capture detector and a mass spectrometer. VOCs characterized include light hydrocarbons, alkyl nitrates, aromatics and some biogenic compounds. This analytical method has been used in several previous studies (Russo et al., 2010a; Swarthout et al., 2013; Zhou et al., 2010).

Meteorological data were collected using Climatronics All-In-One Weather Sensors at THRO-N and FOUS. Meteorological data from MELA and Watford City, ND (8 km from THRO-N) were obtained from the Western Regional Climate Center Remote Automated Weather Stations (RAWS, http://www.raws.dri.edu/index.html), which included solar radiation measured by pyranometers. The interactive snow information dataset from the National Operational Hydrologic Remote Sensing Operation (NOAA, http://www.nohrsc.noaa.gov/interactive/html/map.html) was averaged from two sites in Killdeer, ND (50 km from THRO-N) to eliminate data coverage gaps and used to determine the percentage of days when snow cover was present in the Bakken region. Radiosonde data from atmospheric soundings taken at 00 and 12Z in Bismarck, ND (210 km from THRO-N) were used to investigate atmospheric stability (University of Wyoming, http://weather.uwyo.edu/upperair/sounding.html). The potential temperature method was used to calculate the mixing height (Beyrich and Leps, 2012; Seibert et al., 1997). All site locations where measurements were obtained are shown in Fig. 1.

A sensitivity analysis was performed using the thermodynamic aerosol model ISORROPIA and its adjoint model ANISORROPIA. ANISORROPIA, an inverse sensitivity model (Capps et al., 2012), was used in conjunction with ISORROPIA (Fountoukis and Nenes, 2007; Nenes, 1998) to determine the sensitivities of PM concentrations to changes in aerosol precursor concentration. The input for ISORROPIA, run in the forward mode, included hourly MARGA measurements of total gaseous NH_3 and particulate NH_4^+, total gaseous HNO_3 and particulate NO_3^-, and particulate SO_4^{2-}. The model partitioned total NH_3 and NH_4^+ (N(-III)), total HNO_3 and NO_3^- (N(V)) and total SO_4^{2-} and HSO_4^- into their respective gas and aerosol phase species. The model was run in metastable conditions with no formation of ice or other solid species. No errors were produced from the ISORROPIA model output, but samples that produced errors in the ANISORROPIA model were removed before analysis.

3. Results

Periods of elevated inorganic aerosol concentrations were observed in the URG filter-pack measurements collected during both studies as shown in Fig. 2. Observations from both studies show that increased concentrations occurred regionally across all measurement sites. High concentration episodes were dominated by NH_4^+, SO_4^{2-} and NO_3^-. Concentrations of all other ions measured, including Cl^-, NO_2^-, K^+, Na^+, Ca^{2+}, and Mg^{2+}, were low. The sample number, mean, standard deviation and maximum concentrations of each aerosol species at all sites for both studies are given in Table S3. The highest time-integrated concentration of total inorganic components measured during both studies occurred at FOUS during the first study in late March, which was 21.3 μg m^{-3} for a 48-h sample. FOUS, which was surrounded by a dense area of oil wells, also had the highest average inorganic aerosol concentration during BAQS II. MELA, a study background site located west and often upwind of the Bakken production region, had the lowest average inorganic aerosol concentration during both studies. For the three sites used in both studies (THRO-N, FOUS, and MELA), average inorganic $PM_{2.5}$ concentrations were over two times greater for the entire first study period compared to the entire second study period. This difference was found to be significant using the Student's t-test (Table S4). The mean b_{sp} at THRO-N was also over two times greater during BAQS I compared to BAQS II: 15.3 Mm^{-1} vs 7.1 Mm^{-1}. BC in $PM_{2.5}$ concentrations in BAQS II averaged 0.2 μg m^{-3} with a maximum hourly concentration of 1.9 μg m^{-3}. For BAQS I, BC concentrations averaged 0.2 μg m^{-3} with a maximum hourly concentration of 1.4 μg m^{-3}. Timelines of nephelometer and BC measurements are presented in Figs. S3 and S4.

During BAQS II, additional instrumentation was added to THRO-N to measure organic aerosol and inorganic aerosol at higher time resolution. AMS organic aerosol in PM_1 during BAQS II averaged 1.08 ± 0.66 μg m^{-3} with a maximum hourly concentration of 4.94 μg m^{-3}. The total inorganic aerosol in $PM_{2.5}$ measured by MARGA averaged 2.39 ± 2.32 μg m^{-3} with a maximum hourly concentration of 19.5 μg m^{-3}. The sample number, mean, standard deviation and maximum concentrations of each aerosol species for the MARGA and AMS during BAQS II are given in Table S5. Timelines of AMS and MARGA measurements are presented in Figs. S5 and S6.

The temperature and relative humidity from each study are summarized in Table S6. Only similar time periods from both studies are included in this table in order to facilitate comparison between the two studies without a bias from seasonal differences. The temperature varied slightly between sites, with MELA being between 1.7 and 3.1 °C colder on average than the other two sites for each study period. THRO-N and FOUS had comparable average

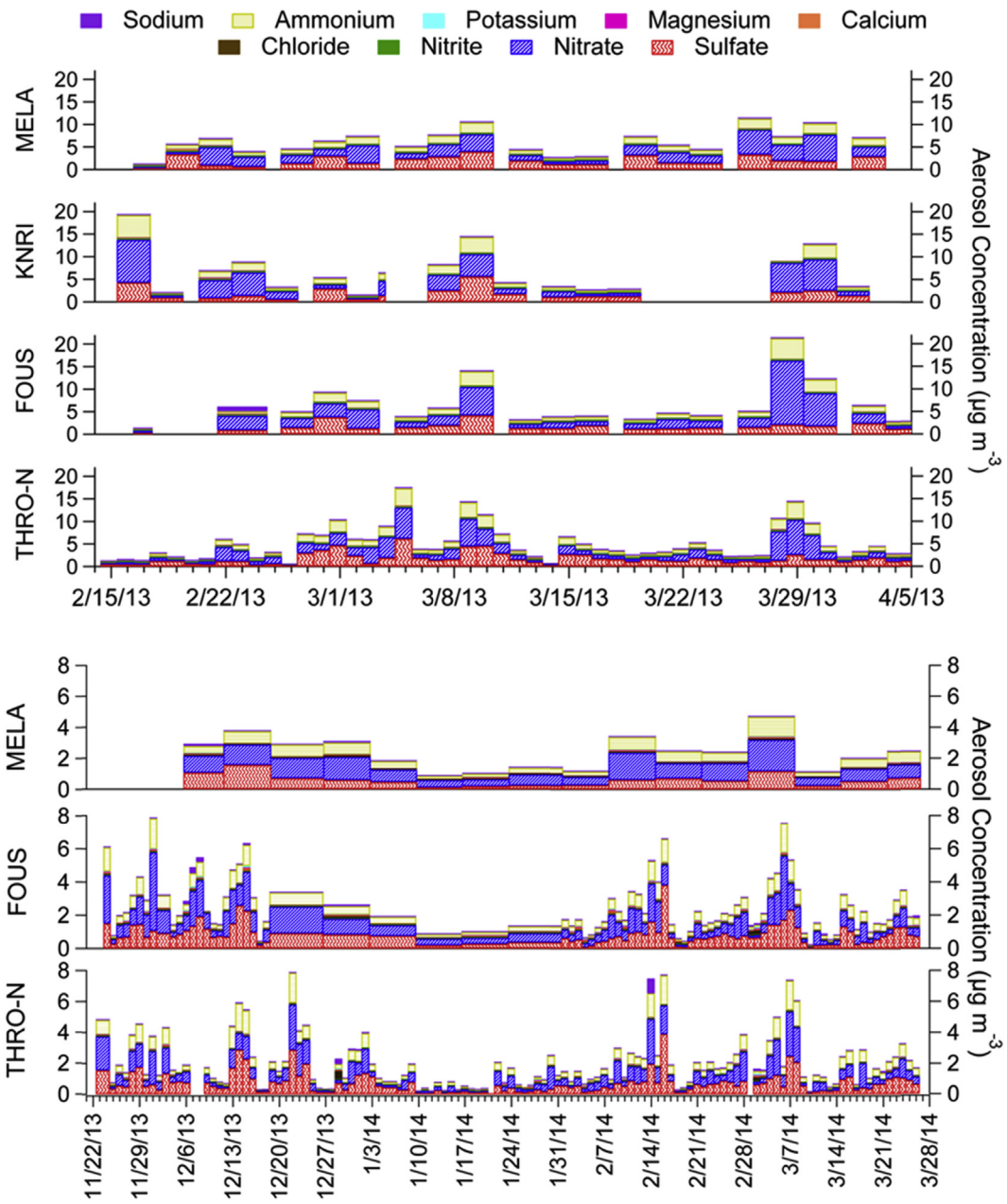

Fig. 2. Stacked bars representing the contribution of each inorganic species to the total inorganic aerosol from URG filter $PM_{2.5}$ measurements (μg m^{-3}) from the first study (top panel) and the second study (bottom panel). The width of the bar signifies the sampling period which varied between daily, 2-day, and weekly samples. Note the different scales for the two studies.

temperatures between both studies. Relative humidity was higher at each site during BAQS I compared to BAQS II. Fig. 3 shows the differences in wind direction and wind speed during the overlapping BAQS I and II time periods. In BAQS I, the wind originated from both the southeast and northwest. BAQS II winds came predominantly from the west northwest, but wind speeds were similar between studies.

4. Discussion

4.1. Study comparison

4.1.1. Influence from meteorology

Comparing overlapping times of year (February 15 through March 28), the average inorganic $PM_{2.5}$ concentrations totaled 5.0 and 2.3 μg m^{-3} at THRO-N in 2013 and 2014, respectively, more than a factor of two difference. Local wind speed and wind direction at THRO-N are plotted in Fig. 3. The mean wind speed was 1.84 m s^{-1} for 2013, slightly higher than the average 1.67 m s^{-1} for 2014. Both years show strong northwesterly flow, but 2013 also has a significant contribution from southeasterly wind. Increased transport of NH_3 from agricultural regions southeast (Pitchford et al., 2009) or north (Carew, 2010) of the Bakken formation might have also helped increase AN formation. No significant differences in average site temperature were observed, but the average relative humidity was lower at all sites during 2014 (Table S6), which could impact AN formation.

Near THRO-N, average solar radiation at 14:00 decreased from 0.59 to 0.44 kW h m^{-2} between BAQS I and II (Fig. S7). Snow cover was present for 89% of BAQS I and only 35% of BAQS II. The presence

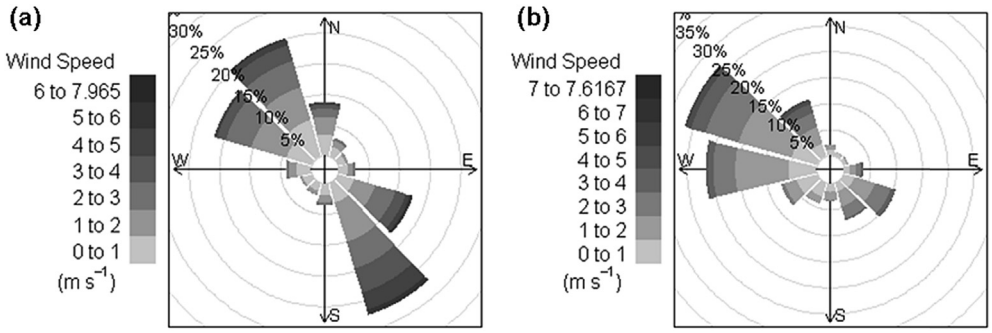

Fig. 3. Wind roses using matching date ranges of February 13 through March 25 from the first study in 2013 (a) and the second study in 2014 (b) from THRO-N. The percent probability that the wind came from each direction is shown by the length of each wedge and is colored by wind speed (m s^{-1}).

of snow cover can intensify solar radiation and enhance photochemistry, which has been shown to generate high concentrations of pollutants such as ozone and particulate nitrate in previous studies (Li et al., 2014; Rappenglück et al., 2014). Snow cover can also strengthen the nighttime inversion layer, trap $PM_{2.5}$ and $PM_{2.5}$ precursor emissions near the surface, and create colder and more humid conditions which are favorable for AN formation (Green et al., 2015). Median atmospheric mixing heights were 293 m and 375 m for 2013 and 2014. Differences in local wind direction, higher relative humidity, higher solar radiation, more persistent snow cover and lower average mixing height during 2013 may all have contributed to the higher $PM_{2.5}$ concentrations observed.

4.1.2. Aerosol source regions and atmospheric age

Regional transport patterns were investigated to better understand source regions of observed pollutants. Back trajectories were produced using the hybrid single particle Lagrangian integrated trajectory model (HYSPLIT; Stein et al., 2015) with meteorological input from North American Regional Reanalysis (NARR) data. A residence time analysis was performed to determine the source regions associated with individual aerosol species; each grid cell is colored by the percentage of air masses that resided in that cell. Fig. 4 shows the residence time of the air masses with the highest 10% of NO_3^- (a and c) and SO_4^{2-} (b and d) concentrations from the daily URG filters for BAQS I (a and b) and MARGA hourly concentrations for BAQS II (c and d). In the first study, the highest concentrations of NO_3^- were associated with transport from southeast of THRO-N while the highest concentrations of SO_4^{2-} are associated with air masses spending time in the Bakken oil patch region as well as in regions to the northwest and northeast. The different patterns suggest that different source regions exist for NO_3^- and SO_4^{2-} precursor emissions. In the second study, the highest concentrations of NO_3^- and SO_4^{2-} do not show clear trends in the residence time analysis, with the exception of significant time spent in the Bakken oil patch region itself. Back trajectories also clearly show patterns of air recirculation and stagnation in the Bakken region during regional $PM_{2.5}$ episodes (Fig. S8). This is similar to the findings of Prenni et al. (2016), who showed that the highest concentrations of aerosol precursors (NO_x and SO_2) during the BAQS study corresponded to trajectories that were shorter (slower speeds) and were more likely to be impacted by closer sources. For comparison, the residence times of trajectories associated with the lowest 10% of NO_3^- and SO_4^{2-} concentrations from the second study and representative back trajectories from a period of low $PM_{2.5}$ concentrations show fast transport solely from the west (Figs. S9 and S8). Analysis of the residence times and local winds from both studies show that the highest concentrations of both NO_3^- and SO_4^{2-} are associated with emissions from nearby THRO-N, suggesting the importance of sources local to the oil production region.

Local winds and measured b_{sp} were examined at FOUS to gain insight as to which source regions are important specifically for the degradation of visibility. A wind rose (Fig. 5a) and conditional probability plot (CPF) showing the 90th percentile b_{sp} concentration (Fig. 5b) show a clear relationship between the highest values of b_{sp} and easterly local winds and light wind speeds. Easterly winds at FOUS, which is located near the western edge of the Bakken region (Fig. 1), originate from the densest area of oil and gas operations which reinforces the importance of local sources on $PM_{2.5}$ concentrations and haze. The major role of local sources also suggests that long range transport, such as from the Alberta oil sands, does not likely significantly contribute to the PM concentrations and haze in the Bakken region.

To further examine whether the highest inorganic aerosol concentrations are influenced by local emissions, a photochemical clock is used to estimate the atmospheric age of emissions in Fig. 6. This plot utilizes the concentrations of 2-pentyl nitrate, 2-butyl nitrate and their parent alkanes obtained from VOC canister measurements at THRO-N. The reaction rates of these alkanes with nitrogen oxides and the chemical evolution of the alkyl nitrates are well known, so the ratio of the parent alkane to its alkyl nitrate can be used as a proxy for time or airmass age (Bertman et al., 1995; Russo et al., 2010b). Overlaid on this plot are the inorganic aerosol concentration (sum of NH_4^+, NO_3^-, and SO_4^{2-}) and the calculated airmass age. The airmass age is estimated to be well under one day when the highest inorganic aerosol concentrations are observed. Fig. 6 also shows i-/n-pentane ratios observed in THRO-N, represented by marker size. The i-/n-pentane ratios from BAQS are described in detail in Prenni et al. (2016). Briefly, the i-/n-pentane ratio has been used in previous oil and gas studies as a marker of urban emissions if the ratio is greater than 1 or oil and gas emissions if the ratio is less than 1 (Gilman et al., 2013; Swarthout et al., 2013). A smaller marker size in Fig. 6 represents a smaller i-/n-pentane ratio, which is indicative of oil and gas emissions. The lower i-/n-pentane ratios correspond with both higher $PM_{2.5}$ concentrations and younger air mass age. Combined with the preceding transport analysis, this is compelling evidence that emissions from local sources from oil and gas operations are large contributors to the high concentration aerosol episodes observed.

4.2. Aerosol composition and formation

4.2.1. $PM_{2.5}$ speciation at THRO-N

An investigation of the higher time resolved aerosol measurements from BAQS II is presented here. Limitations in deployed instrumentation prevent the same analysis for BAQS I. However,

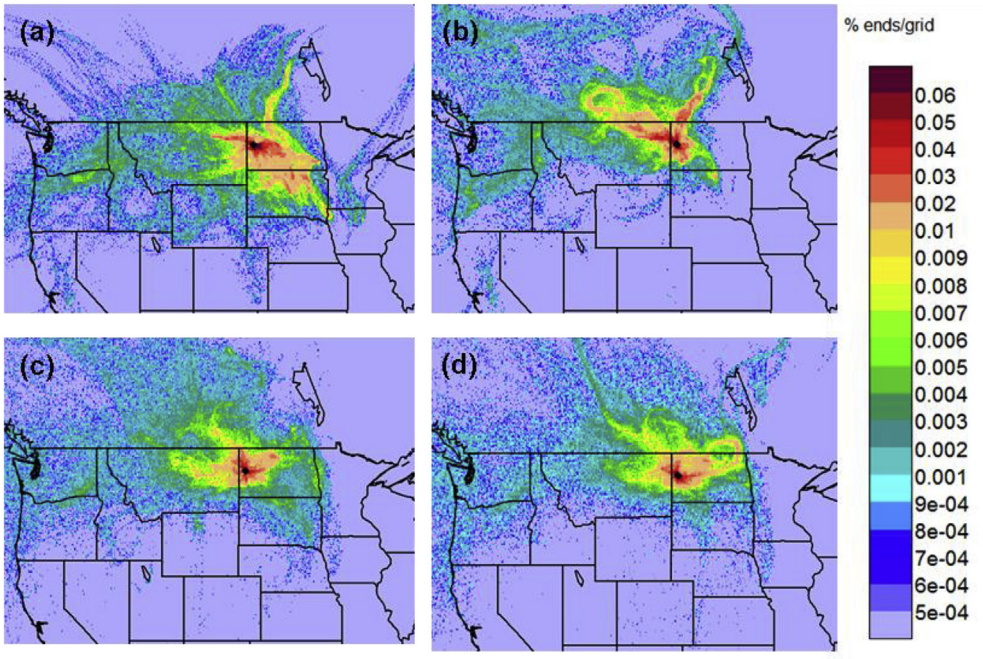

Fig. 4. The residence times of the highest 10% concentrations using five day ensemble trajectories of nitrate (panels a and c) and sulfate (panels b and d) using URG measurements during the first study from 2/14/13–4/5/13 (top panels) and using MARGA measurements during the second study from 11/30/13–3/24/14 (bottom panels).

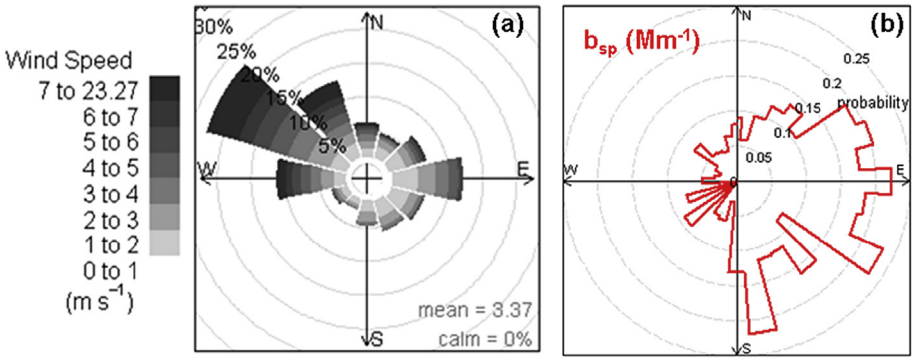

Fig. 5. A wind rose (a) and conditional probability function plot (CPF, b) are shown from FOUS from the second study. The CPF plot shows the wind directions associated with the 90th percentile concentrations of b_{sp} (31.6 Mm^{-1}) and the probability of occurrence.

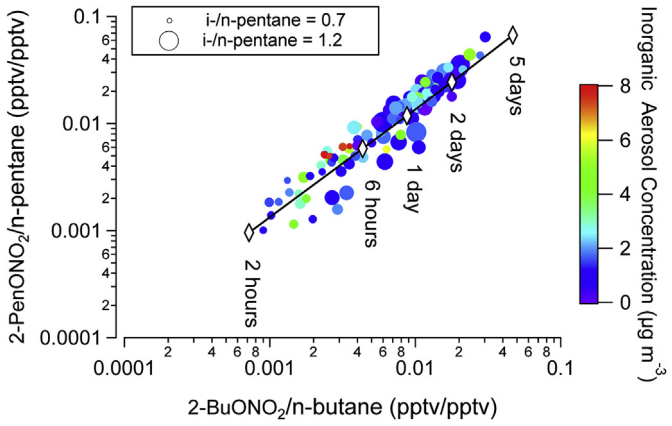

Fig. 6. The alkyl nitrate chemical clock (see text for description) shows the estimated age of VOC emissions in the sampled air mass and is overlaid with the total inorganic aerosol concentration from URG measurements and the i-/n-pentane ratio.

similar trends in the episodic nature of the elevated regional $PM_{2.5}$ concentrations, a similar rate of oil production (Fig. S1), and a similar average ratio of $PM_{2.5}$ nitrate to sulfate were observed in both studies. The comparable emissions and aerosol chemistry in both studies suggests that the speciation results observed for BAQS II are representative of BAQS I. For this analysis, we use hourly reconstructed $PM_{2.5}$ mass which is calculated from the sum of the inorganic species in $PM_{2.5}$ from the MARGA, total organics in PM_1 from the AMS (we assume that organic mass is mostly below 1 μm) and BC in $PM_{2.5}$ from the aethalometer. To determine that a significant amount of $PM_{2.5}$ organic aerosol was not missing in our PM_1 measurement, AMS PM_1 organic carbon (OC) and IMPROVE $PM_{2.5}$ OC were compared (Fig. S10). The average ratio and standard deviation of AMS PM_1 OC to IMPROVE $PM_{2.5}$ OC was 1.1 ± 0.6, indicating that the AMS PM_1 measurement is similar to the $PM_{2.5}$ organic mass. Additional comparisons of the carbonaceous, inorganic, and total PM measurements are presented in Figs. S10, S11 and S12. For further validation, the IMPROVE total $PM_{2.5}$ mass compared to the reconstructed $PM_{2.5}$ mass has a slope of 1.0, y-

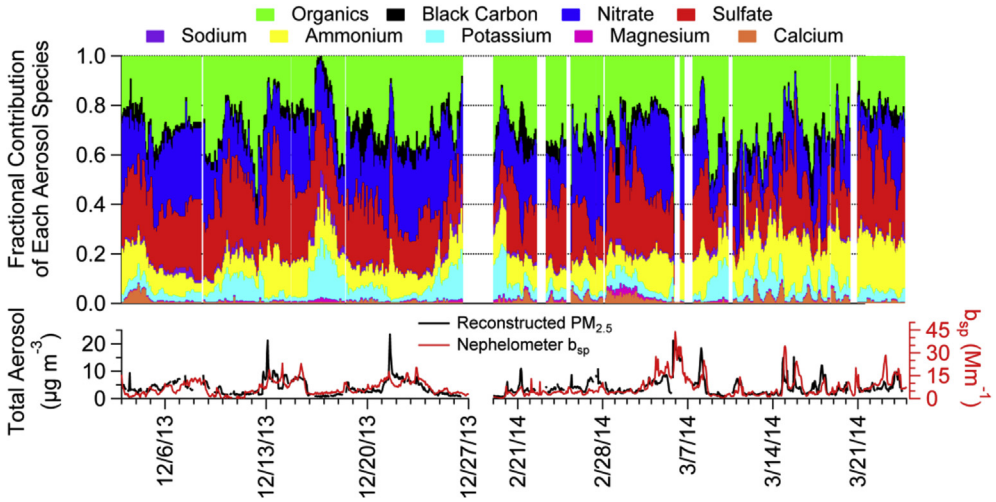

Fig. 7. The top panel is a timeline of the fraction of each inorganic species, total organics and black carbon that contribute to total hourly reconstructed $PM_{2.5}$ mass. The bottom timeline shows the reconstructed $PM_{2.5}$ mass ($\mu g\ m^{-3}$) and the total light extinction due to particle scattering (b_{sp}) from nephelometer measurements (Mm^{-1}).

intercept of −0.41 and a R^2 of 0.92 (Fig. S12), indicating that the reconstructed $PM_{2.5}$ is representative of the total measured $PM_{2.5}$ mass observed during the study.

The fraction of each aerosol component and reconstructed $PM_{2.5}$ concentration represented as the sum of all measured components are shown in Fig. 7. On average, inorganics contribute 64.9%, organics contribute 29.7%, and BC contributes 5.4% to the total $PM_{2.5}$ mass. During periods of elevated aerosol concentration, the inorganic species dominate the aerosol fraction and in particular the contribution from NO_3^- increases. Between the lowest and highest $PM_{2.5}$ mass quartiles, the fraction of NO_3^- increases from 15% to 32% while the fraction of SO_4^{2-} only increases from 18 to 22% (Fig. S13) indicating a greater importance of AN formation at higher total $PM_{2.5}$ concentrations. Differences between NO_3^- and SO_4^{2-} source regions will be discussed below. Fig. 7 also shows that b_{sp} measured by the nephelometer tracks closely with total $PM_{2.5}$ mass.

4.2.2. Role of aerosol precursor gases in inorganic particle formation

In the atmosphere, emissions of SO_2 can oxidize to form sulfuric acid (H_2SO_4) which readily condenses into the particle phase. In the presence of NH_3, AS aerosol will form preferentially. If excess N(-III) exists, AN can form (Seinfeld and Pandis, 2006). Excess N(-III) can be calculated using Equation (1), by subtracting twice the measured particulate SO_4^{2-} from total N(-III), with all concentrations in molar units. When excess N(-III) is present, formation of AN is highly dependent on temperature and relative humidity and is favored in cold and humid conditions (Stelson and Seinfeld, 1982), as were present during both studies. Equation (1) represents a lower bound on excess N(-III) concentrations based on work by Silvern et al. (2016) and Weber et al. (2016) who suggest that in some regions, excess N(-III) can exist despite incomplete neutralization of SO_4^{2-}.

$$[N(-III)]_{excess} = \left[NH_4^+\right] + [NH_3] - 2^*\left[SO_4^{2-}\right] \quad (1)$$

Concentration timelines of total N(-III) species and total N(V) species are plotted in Fig. 8. The color of the line indicates the gas fraction of NH_3 or HNO_3 relative to the total N(-III) or N(V), ranging from 0 (all N(-III) or N(V) in particulate form) to 1 (all N(-III) or N(V) in the gas phase). During the majority of periods with high concentrations of N(V) and N(-III), the gas fractions were low, indicating both N(-III) and N(V) were predominantly in the particle phase. The NH_3 gas fraction is higher during the beginning and end of the study, when temperatures were also generally higher. December and March, for example, featured average NH_3 gas fractions and temperatures of 0.2 and −8 °C and 0.5 and −1 °C, respectively. The average HNO_3 gas ratio was 0.3 for both December and March. This reveals that periods with extremely cold temperatures are often limited by NH_3 while throughout the entire winter study period there is limited HNO_3 available. Increases in excess N(-III) in March may reflect NH_3 emission from the application of fertilizer or other regional agricultural practices in combination with warmer temperatures which increases NH_3 volatilization (Balasubramanian et al., 2015; Gilliland et al., 2006).

The sensitivity of AN and $PM_{2.5}$ formation to sulfate, N(-III), and N(V) concentrations investigated using ANISORROPIA is summarized in Table 1. Understanding how further growth in regional NO_x emissions, which are likely to yield increases in HNO_3 concentrations, might impact AN formation is of particular interest in contemplating possible effects from future growth in Bakken oilfield development on regional haze. The average sensitivities of inorganic NO_3^- formation, for example, to changes in total N(-III) and N(V) concentrations are listed in Table 1 as 0.36 and 0.13, respectively. These values indicate that, on average, a 1 mol increase in total N(-III) would yield a 0.36 mol increase in $PM_{2.5}$ NO_3^-, while a 1 mol increase in total N(V) would yield a smaller, 0.13, mole increase in $PM_{2.5}$ NO_3^-. This suggests that the formation of particulate matter is more sensitive to increases in NH_3 than to increases in NO_x during the winter months, when the input data were collected. The average sensitivities of $PM_{2.5}$ NH_4^+ to changes in N(-III) and N(V) are 0.76 and 0.11 mol/mole. Concentrations of SO_4^{2-}, by contrast, are seen to be relatively insensitive to changes in N(-III) or N(V), due to the low volatility of SO_4^{2-} which keeps it predominantly in the aerosol phase. The sensitivities of inorganic $PM_{2.5}$ concentrations to changes in N(-III) and N(V) ($\mu g/\mu g$) are explored in more detail in Fig. 9. Here we see that the sensitivity of total $PM_{2.5}$ concentrations to N(-III) is typically greater during colder periods when excess N(-III) is low, indicating the strong limitation of fine particle formation imposed by NH_3 during these times. At warmer temperatures during late winter, excess N(-III) increases and the sensitivity of $PM_{2.5}$ formation to N(-III) is generally low. Not surprisingly, a contrasting trend is seen for $PM_{2.5}$ sensitivity to N(V). Fig. 9b shows that $PM_{2.5}$ is not very sensitive to N(V) concentrations at extremely low temperatures and low excess N(-III)

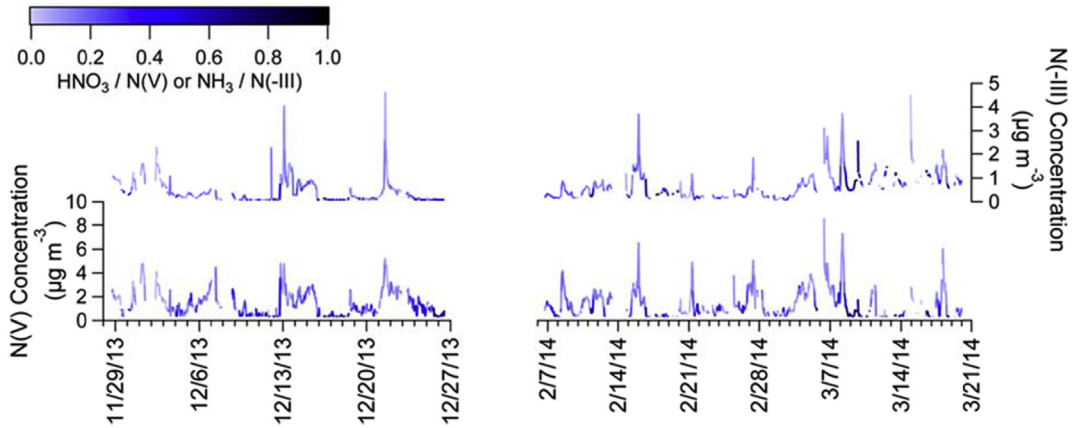

Fig. 8. N(-III) and N(V) concentrations (μg m^{-3}) observed in the second study at THRO-N using hourly MARGA measurements. The timeline color indicates the N(-III) gas ratio (NH_3/N(-III)) and N(V) gas ratio (HNO_3/N(V)). (For interpretation of the references to colour in this figure legend, the reader is referred to the web version of this article.)

Table 1
Study averaged model sensitivities (bold) and standard deviation (in parentheses) for the formation of particulate species H^+, NO_3^-, NH_4^+, SO_4^{2-}, HSO_4^- and total $PM_{2.5}$. Sensitivities to individual species are given as a molar ratio of the model predicted aerosol species over the input of total N(-III), N(V) or SO_4^{2-}. The sensitivity of predicted total $PM_{2.5}$ was calculated by summing the sensitivities of each predicted aerosol species to the three different input species and is given in mass units (μg/μg).

δ predicted/δ input	δH^+	δNO_3^-	δNH_4^+	δSO_4^{2-}	δHSO_4^-	$\delta PM_{2.5}$
	(mole/mole)					(μg/μg)
δN(-III)	**−0.37** (0.44)	**0.36** (0.42)	**0.76** (0.40)	**0.02** (0.05)	**−0.02** (0.05)	**1.99** (1.64)
δN(V)	**0.02** (0.04)	**0.13** (0.25)	**0.11** (0.25)	**−0.002** (0.01)	**0.001** (0.006)	**0.17** (0.32)
δSO_4^{2-}	**0.81** (0.85)	**−0.60** (0.78)	**0.51** (0.84)	**0.96** (0.11)	**0.04** (0.11)	**0.72** (0.59)

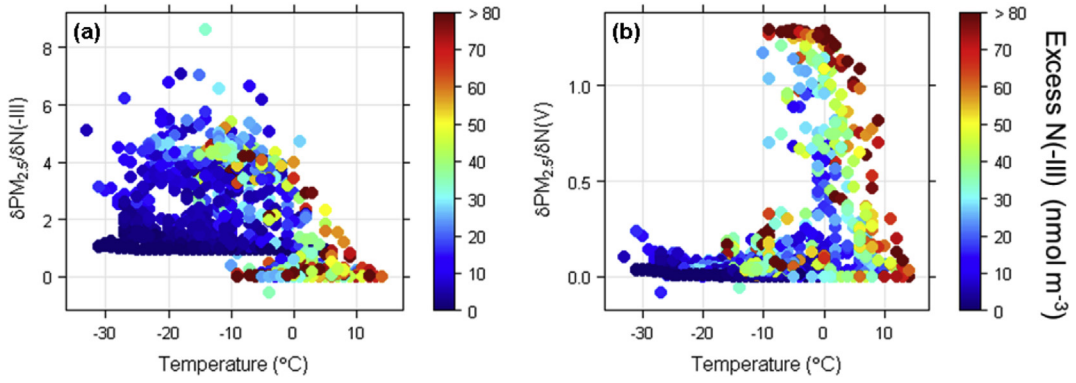

Fig. 9. The sensitivities of $PM_{2.5}$ to N(-III) and N(V) concentrations (μg/μg) calculated by ANISORROPIA. Panel (a) shows the sensitivity of $PM_{2.5}$ to N(-III) and panel (b) shows the sensitivity of $PM_{2.5}$ to N(V) compared with temperature in °C on the x-axis; the points are colored by the concentrations of excess N(-III) in nmol m^{-3}.

concentrations, but that the sensitivity sharply increases above −10 °C when excess N(-III) concentrations tend to be higher. These findings suggest that effects of additional future NO_x emissions from additional oil development activities in the region are likely to exert the strongest effects on haze formation during later parts of winter when temperatures and NH_3 concentrations increase.

5. Conclusion

Intensive ground-based aerosol measurements over two consecutive winters in the Bakken oil and gas region showed periods of regionally elevated concentrations of $PM_{2.5}$, with a maximum 48-h average $PM_{2.5}$ inorganic aerosol concentration of 21.3 μg m^{-3} observed at Fort Union in the heart of the Bakken oil patch. The lowest concentrations were typically found at Medicine Lake, outside and often upwind of the oil patch. Concentrations across the region were found to be highest during periods of air mass stagnation and recirculation; the lowest concentrations were typically associated with fast transport of air from the west or northwest. Both average and peak $PM_{2.5}$ concentrations were higher in early 2013 than in early 2014. Differences in snow cover, atmospheric stability, solar illumination, and transport directions might be associated with the differing fine particle concentrations and aerosol scattering measurements. Use of a chemical clock revealed that periods with the highest $PM_{2.5}$ concentrations tended to be associated with VOC emissions aged less than a day and a VOC signature more indicative of oil and gas contributions than from urban centers. This reinforces the importance of local Bakken region sources in formation of regional haze episodes.

Inorganic species made up the majority of the total $PM_{2.5}$ mass, with both ammonium sulfate and ammonium nitrate having significant contributions. We observed increases in NO_x emitted from oil and gas operations (Prenni et al., 2016), which formed HNO_3 and combined with available NH_3 to form ammonium nitrate aerosol and contributed to haze episodes. It was shown using meteorological conditions, gas and aerosol measurements, and thermodynamic modeling, that conditions in the Bakken were favorable for ammonium nitrate formation for the majority of the sampling period. $PM_{2.5}$ concentrations were typically more sensitive to the availability of N(-III) during the coldest part of the winter; sensitivity to available N(V) grew as temperatures increased along with N(-III) availability in the later part of winter.

Acknowledgements

The Bakken Air Quality Study was funded by the National Park Service. This publication was developed with additional support from STAR Fellowship Assistance Agreement No. FP917705 awarded by the U.S. Environmental Protection Agency to Ashley Evanoski-Cole. It has not been formally reviewed by EPA. The views expressed in this publication are solely those of the authors, and EPA does not endorse any products or commercial services mentioned in this publication. The assumptions, findings, conclusions, judgements, and views presented herein are those of the authors and should not be interpreted as necessarily representing official National Park Service policies. The authors acknowledge the generous support from the staff at Theodore Roosevelt National Park, Knife River Indian Villages National Historic Site, Fort Union Trading Post National Historic Site and Medicine Lake National Wildlife Refuge. Steven Brey is also gratefully acknowledged for his expertise in R and help with developing code to analyze the atmospheric soundings. S. Capps gratefully acknowledges support from the National Science Foundation through the AirWaterGas Sustainability Research Network.

Appendix A. Supplementary data

Supplementary data related to this article can be found at http://dx.doi.org/10.1016/j.atmosenv.2017.02.019.

References

Balasubramanian, S., Koloutsou-vakakis, S., Mcfarland, D.M., Rood, M.J., 2015. Reconsidering emissions of ammonia from chemical fertilizer usage in Midwest USA. J. Geophys. Res. Atmos. 1–15. http://dx.doi.org/10.1002/2015JD023219.Received.

Bar-Ilan, A., Friesen, R., Grant, J., Pollack, A., Henderer, D., Pring, D., Sgamma, K., Moore, T., 2008. A Comprehensive Oil and Gas Emissions Inventory for the Denver-Julesburg Basin in Colorado (Environ Report. Novato, CA).

Benedict, K.B., Day, D., Schwandner, F.M., Kreidenweis, S.M., Schichtel, B., Malm, W.C., Collett, J.L., 2013. Observations of atmospheric reactive nitrogen species in Rocky Mountain National Park and across northern Colorado. Atmos. Environ. 64, 66–76. http://dx.doi.org/10.1016/j.atmosenv.2012.08.066.

Bertman, S.B., Roberts, J.M., Parrish, D.D., Buhr, M.P., Goldan, P.D., Kuster, W.C., Fehsenfeld, F.C., Montzka, S.A., Westberg, H., 1995. Evolution of alkyl nitrates with air mass age. J. Geophys. Res. 100, 22805. http://dx.doi.org/10.1029/95JD02030.

Beyrich, F., Leps, J.-P., 2012. An operational mixing height data set from routine radiosoundings at Lindenberg: methodology. Meteor. Z. 21, 337–348. http://dx.doi.org/10.1127/0941-2948/2012/0333.

Capps, S.L., Henze, D.K., Hakami, A., Russell, A.G., Nenes, A., 2012. ANISORROPIA: the adjoint of the aerosol thermodynamic model ISORROPIA. Atmos. Chem. Phys. 12, 527–543. http://dx.doi.org/10.5194/acp-12-527-2012.

Carew, R., 2010. Ammonia emissions from livestock industries in Canada: feasibility of abatement strategies. Environ. Pollut. 158, 2618–2626. http://dx.doi.org/10.1016/j.envpol.2010.05.004.

Choi, J., Roberts, D.C., 2015. Impacts of air pollution on productivity growth in the air and truck transportation industries in the US: an application of the data envelopment analysis malmquist environmental productivity index. Open J. Soc. Sci. 3, 120–129.

Chow, J.C., Watson, J.G., Chen, L.-W.A., Chang, M.C.O., Robinson, N.F., Trimble, D., Kohl, S., 2007. The IMPROVE_A temperature protocol for thermal/optical carbon analysis: maintaining consistency with a long-term database. J. Air Waste Manage. Assoc. 57, 1014–1023. http://dx.doi.org/10.3155/1047-3289.57.9.1014.

Decarlo, P.F., Kimmel, J.R., Trimborn, A., Northway, M.J., Jayne, J.T., Aiken, A.C., Gonin, M., Fuhrer, K., Horvath, T., Docherty, K.S., Worsnop, D.R., Jimenez, J.L., 2006. Field-deployable, high-resolution, time-of-flight aerosol mass spectrometer. Anal. Chem. 78, 8281–8289 doi:8410.1029/2001JD001213.

Drewnick, F., Hings, S.S., DeCarlo, P., Jayne, J.T., Gonin, M., Fuhrer, K., Weimer, S., Jimenez, J.L., Demerjian, K.L., Borrmann, S., Worsnop, D.R., 2005. A new time-of-flight aerosol mass spectrometer (TOF-AMS) - instrument description and first field deployment. Aerosol Sci. Technol. 39, 637–658. http://dx.doi.org/10.1080/02786820500182040.

Drinovec, L., Močnik, G., Zotter, P., Prévôt, A.S.H., Ruckstuhl, C., Coz, E., Rupakheti, M., Sciare, J., Müller, T., Wiedensohler, A., Hansen, A.D.A., 2015. The "dual-spot" Aethalometer: an improved measurement of aerosol black carbon with real-time loading compensation. Atmos. Meas. Tech. 8, 1965–1979. http://dx.doi.org/10.5194/amt-8-1965-2015.

Fountoukis, C., Nenes, A., 2007. ISORROPIA II: a computationally efficient thermodynamic equilibrium model for K+–Ca2+–Mg2+–NH4+–Na+–SO42––NO3––Cl––H2O aerosols. Atmos. Chem. Phys. 7, 4639–4659. http://dx.doi.org/10.5194/acp-7-4639-2007.

Gaswirth, S.B., Marra, K.R., 2015. U.S. geological survery 2013 assessment of undiscovered resources in the Bakken and three Forks formations of the U.S. Williston basin province. Am. Assoc. Pet. Geol. Bull. 99, 639–660.

Gilliland, A.B., Wyat Appel, K., Pinder, R.W., Dennis, R.L., 2006. Seasonal NH3 emissions for the continental United States: inverse model estimation and evaluation. Atmos. Environ. 40, 4986–4998. http://dx.doi.org/10.1016/j.atmosenv.2005.12.066.

Gilman, J.B., Lerner, B.M., Kuster, W.C., de Gouw, J.A., 2013. Source signature of volatile organic compounds from oil and natural gas operations in northeastern Colorado. Environ. Sci. Technol. 47, 1297–1305. http://dx.doi.org/10.1021/es304119a.

Giwa, S.O., Adama, O.O., Akinyemi, O.O., 2014. Baseline black carbon emissions for gas flaring in the Niger Delta region of Nigeria. J. Nat. Gas. Sci. Eng. 20, 373–379. http://dx.doi.org/10.1016/j.jngse.2014.07.026.

Grant, J., Parikh, R., Bar-Ilan, A., Morris, R., 2014a. Development of Baseline 2011 and Future Year 2015 Emissions from Oil and Gas Activity in the Williston Basin (Environ Report. Novato, CA).

Grant, J., Parikh, R., Bar-Ilan, A., Morris, R., 2014b. Development of Baseline 2011 and Future Year 2015 Emissions from Oil and Gas Activity in the Great Plains Basin (Environ Report. Novato, CA).

Green, M.C., Chow, J.C., Watson, J.G., Dick, K., Inouye, D., 2015. Effects of snow cover and atmospheric stability on winter $PM_{2.5}$ concentrations in western U.S. Valleys. J. Appl. Meteorol. Climatol. 54, 1191–1201. http://dx.doi.org/10.1175/JAMC-D-14-0191.1.

Hand, J.L., 2011. Spatial and Seasonal Patterns and Temporal Variability of Haze and its Constituents in the United States (IMPROVE Report V. Fort Collins, CO).

Hand, J.L., Gebhart, K.A., Schichtel, B.A., Malm, W.C., 2012. Increasing trends in wintertime particulate sulfate and nitrate ion concentrations in the Great Plains of the United States (2000–2010). Atmos. Environ. 55, 107–110. http://dx.doi.org/10.1016/j.atmosenv.2012.03.050.

Hansen, A.D.A., Rosen, H., Novakov, T., 1984. The aethalometer — an instrument for the real-time measurement of optical absorption by aerosol particles. Sci. Total Environ. 36, 191–196. http://dx.doi.org/10.1016/0048-9697(84)90265-1.

Heintzenberg, J., Wiedensohler, A., Tuch, T.M., Covert, D.S., Sheridan, P., Ogren, J.A., Gras, J., Nessler, R., Kleefeld, C., Kalivitis, N., Aaltonen, V., Wilhelm, R.T., Havlicek, M., 2006. Intercomparisons and aerosol calibrations of 12 commercial integrating nephelometers of three manufacturers. J. Atmos. Ocean. Technol. 23, 902–914. http://dx.doi.org/10.1175/JTECH1892.1.

Jayne, J.T., Leard, D.C., Zhang, X., Davidovits, P., Smith, K.A., Kolb, C.E., Worsnop, D.R., 2000. Development of an aerosol mass spectrometer for size and composition analysis of submicron particles. Aerosol Sci. Technol. 33, 49–70. http://dx.doi.org/10.1080/027868200410840.

Khalek, I.A., Blanks, M.G., Merritt, P.M., Zielinska, B., 2015. Regulated and unregulated emissions from modern 2010 emissions-compliant heavy-duty on-highway diesel engines. J. Air Waste Manage. Assoc. 65, 987–1001. http://dx.doi.org/10.1080/10962247.2015.1051606.

Khlystov, A., Wyers, G.P., Slanina, J., 1995. The steam-jet aerosol collector. Atmos. Environ. 29, 2229–2234 doi:1352-2310(95) 00180–8.

Lee, L., Wooldridge, P.J., Gilman, J.B., Warneke, C., de Gouw, J., Cohen, R.C., 2014. Low temperatures enhance organic nitrate formation: evidence from observations in the 2012 Uintah Basin winter ozone study. Atmos. Chem. Phys. 14, 12441–12454. http://dx.doi.org/10.5194/acp-14-12441-2014.

Lee, T., Yu, X.Y., Ayres, B., Kreidenweis, S.M., Malm, W.C., Collett, J.L., 2008. Observations of fine and coarse particle nitrate at several rural locations in the United States. Atmos. Environ. 42, 2720–2732. http://dx.doi.org/10.1016/j.atmosenv.2007.05.016.

Li, Y., Schwandner, F.M., Sewell, H.J., Zivkovich, A., Tigges, M., Raja, S., Holcomb, S., Molenar, J.V., Sherman, L., Archuleta, C., Lee, T., Collett, J.L., 2014. Observations of ammonia, nitric acid, and fine particles in a rural gas production region. Atmos. Environ. 83, 80–89. http://dx.doi.org/10.1016/j.atmosenv.2013.10.007.

Liggio, J., Li, S., Hayden, K., Taha, Y.M., Stroud, C., Darlington, A., Drollette, B.D., Gordon, M., Lee, P., Liu, P., Leithead, A., Moussa, S.G., Wang, D., O'Brien, J., Mittermeier, R.L., Brook, J.R., Lu, G., Staebler, R.M., Han, Y., Tokarek, T.W.,

Osthoff, H.D., Makar, P.A., Zhang, J., Plata, D.L., Gentner, D.R., 2016. Oil sands operations as a large source of secondary organic aerosols. Nature 534, 91–94. http://dx.doi.org/10.1038/nature17646.

Makkonen, U., Virkkula, A., Hellén, H., Hemmilä, M., Sund, J., Äijälä, M., Ehn, M., Junninen, H., Keronen, P., Petäjä, T., Worsnop, D.R., Kulmala, M., Hakola, H., 2014. Semi-continuous gas and inorganic aerosol measurements at a boreal forest site: seasonal and diurnal cycles of NH3, HONO and HNO3. Boreal Environ. Res. 19, 311–328.

Malm, W.C., 2004. Spatial and monthly trends in speciated fine particle concentration in the United States. J. Geophys. Res. 109 http://dx.doi.org/10.1029/2003JD003739.

Malm, W.C., Schichtel, B.A., Pitchford, M.L., 2011. Uncertainties in PM2.5 gravimetric and speciation measurements and what we can learn from them. J. Air Waste Manage. Assoc. 61, 1131–1149. http://dx.doi.org/10.1080/10473289.2011.603998.

McLinden, C. a., Fioletov, V., Boersma, K.F., Krotkov, N., Sioris, C.E., Veefkind, J.P., Yang, K., 2012. Air quality over the Canadian oil sands: a first assessment using satellite observations. Geophys. Res. Lett. 39 http://dx.doi.org/10.1029/2011GL050273 n/a-n/a.

Müller, T., Nowak, A., Wiedensohler, A., Sheridan, P., Laborde, M., Covert, D.S., Marinoni, A., Imre, K., Henzing, B., Roger, J.-C., Martins dos Santos, S., Wilhelm, R., Wang, Y.-Q., de Leeuw, G., 2009. Angular illumination and truncation of three different integrating nephelometers: implications for empirical, size-based corrections. Aerosol Sci. Technol. 43, 581–586. http://dx.doi.org/10.1080/02786820902798484.

Nenes, A., 1998. ISORROPIA: a new thermodynamic equilibrium model for multiphase multicomponent inorganic aerosols. Aquat. Geochem. 4, 123–152.

Pitchford, M.L., Poirot, R.L., Schichtel, B.a, Malm, W.C., Maim, W.C., 2009. Characterization of the winter midwestern particulate nitrate bulge. J. Air Waste Manage. Assoc. 59, 1061–1069. http://dx.doi.org/10.3155/1047-3289.59.9.1061.

Prenni, A.J., Day, D.E., Evanoski-Cole, A.R., Sive, B.C., Hecobian, A., Zhou, Y., Gebhart, K.A., Hand, J.L., Sullivan, A.P., Li, Y., Schurman, M.I., Desyaterik, Y., Malm, W.C., Schichtel, B.A., Collett Jr., J.L., 2016. Oil and gas impacts on air quality in federal lands in the Bakken region: an overview of the Bakken air quality study and first results. Atmos. Chem. Phys. 16, 1401–1416. http://dx.doi.org/10.5194/acpd-15-28749-2015.

Rappenglück, B., Ackermann, L., Alvarez, S., Golovko, J., Buhr, M., Field, R. a., Soltis, J., Montague, D.C., Hauze, B., Adamson, S., Risch, D., Wilkerson, G., Bush, D., Stoeckenius, T., Keslar, C., 2014. Strong wintertime ozone events in the Upper Green River basin, Wyoming. Atmos. Chem. Phys. 14, 4909–4934. http://dx.doi.org/10.5194/acp-14-4909-2014.

Rumsey, I.C., Cowen, K.A., Walker, J.T., Kelly, T.J., Hanft, E.A., Mishoe, K., Rogers, C., Proost, R., Beachley, G.M., Lear, G., Frelink, T., Otjes, R.P., 2014. An assessment of the performance of the Monitor for AeRosols and GAses in ambient air (MARGA): a semi-continuous method for soluble compounds. Atmos. Chem. Phys. 14, 5639–5658. http://dx.doi.org/10.5194/acp-14-5639-2014.

Russo, R.S., Zhou, Y., Haase, K.B., Wingenter, O.W., Frinak, E.K., Mao, H., Talbot, R.W., Sive, B.C., 2010a. Temporal variability, sources, and sinks of C1 -C5 alkyl nitrates in coastal New England. Atmos. Chem. Phys. 10, 1865–1883.

Russo, R.S., Zhou, Y., White, M.L., Mao, H., Talbot, R., Sive, B.C., 2010b. Multi-year (2004–2008) record of nonmethane hydrocarbons and halocarbons in New England: seasonal variations and regional sources. Atmos. Chem. Phys. 10, 4909–4929. http://dx.doi.org/10.5194/acp-10-4909-2010.

Schurman, M.I., Lee, T., Desyaterik, Y., Schichtel, B.A., Kreidenweis, S.M., Collett, J.L., 2015a. Transport, biomass burning, and in-situ formation contribute to fine particle concentrations at a remote site near Grand Teton National Park. Atmos. Environ. 112, 257–268. http://dx.doi.org/10.1016/j.atmosenv.2015.04.043.

Schurman, M.I., Lee, T., Sun, Y., Schichtel, B.A., Kreidenweis, S.M., Collett, J.L., 2015b. Investigating types and sources of organic aerosol in Rocky Mountain National Park using aerosol mass spectrometry. Atmos. Chem. Phys. 15, 19875–19915. http://dx.doi.org/10.5194/acpd-14-19875-2014.

Seibert, P., Beyrich, F., Gryning, S.-E., Joffre, S., Rasmussen, A., Tercier, P., 1997. Mixing Height Determination for Dispersion Modelling, Preprocessing of Meteorological Data for Dispersion Modelling. Report of Working Group. 2.

Seinfeld, J.H., Pandis, S.N., 2006. Atmospheric Chemistry and Physics: from Air Pollution to Climate Change, Second. ed. Wiley, Hoboken, New Jersey.

Silvern, R.F., Jacob, D.J., Kim, P.S., Marais, E.A., Turner, J.R., 2016. Incomplete sulfate aerosol neutralization despite excess ammonia in the eastern US: a possible role of organic aerosol. Atmos. Chem. Phys. Discuss. 0, 1–21. http://dx.doi.org/10.5194/acp-2016-315.

Slanina, J., ten Brink, H.M., Otjes, R.P., Even, A., Jongejan, P., Khlystov, A., Waijers-Ijpelaan, A., Hu, M., 2001. The continuous analysis of nitrate and ammonium in aerosols by the steam jet aerosol collector (SJAC): extension and validation of the methodology. Atmos. Environ. 35, 2319–2330. http://dx.doi.org/10.1016/s1352-2310(00)00556-2.

Stein, A.F., Draxler, R.R., Rolph, G.D., Stunder, B.J.B., Cohen, M.D., Ngan, F., 2015. NOAA's hysplit atmospheric transport and dispersion modeling system. Bull. Am. Meteorol. Soc. 96, 2059–2077. http://dx.doi.org/10.1175/BAMS-D-14-00110.1.

Stelson, A.W., Seinfeld, J.H., 1982. Relative humidity and temperature dependence of the ammonium nitrate dissociation constant. Atmos. Environ. 16, 983–992. http://dx.doi.org/10.1016/0004-6981(82)90184-6.

Stohl, A., Klimont, Z., Eckhardt, S., Kupiainen, K., Shevchenko, V.P., Kopeikin, V.M., Novigatsky, A.N., 2013. Black carbon in the Arctic: the underestimated role of gas flaring and residential combustion emissions. Atmos. Chem. Phys. 13, 8833–8855. http://dx.doi.org/10.5194/acp-13-8833-2013.

Swarthout, R.F., Russo, R.S., Zhou, Y., Hart, A.H., Sive, B.C., 2013. Volatile organic compound distributions during the NACHTT campaign at the Boulder Atmospheric Observatory: influence of urban and natural gas sources. J. Geophys. Res. Atmos. 118, 10,614–10,637. http://dx.doi.org/10.1002/jgrd.50722.

Trebs, I., Meixner, F.X., Slanina, J., Otjes, R., Jongejan, P., Andreae, M.O., 2004. Real-time measurements of ammonia, acidic trace gases and water-soluble inorganic aerosol species at a rural site in the Amazon Basin. Atmos. Chem. Phys. 4, 967–987.

U.S. Energy Information Administration, 2016. Natural Gas Flaring in North Dakota Has Declined Sharply since 2014 [WWW Document]. Today in Energy. http://www.eia.gov/todayinenergy/detail.cfm?id=26632 (Accessed 8 March 16).

U.S. Energy Information Administration, 2014a. Nonmarketed Natural Gas in North Dakota Still Rising Due to Higher Total Production [WWW Document]. Today in Energy. http://www.eia.gov/todayinenergy/detail.cfm?id=15511 (Accessed 1.January.15).

U.S. Energy Information Administration, 2014b. Bakken Fuels North Dakota's Oil Production Growth [WWW Document]. Today in Energy. http://www.eia.gov/todayinenergy/detail.cfm?id=17391 (Accessed 1 May 15).

U.S. Environmental Protection Agency, 2012. Report to Congress on Black Carbon. Research Triangle Park, NC.

Weber, R.J., Guo, H., Russell, A.G., Nenes, A., 2016. High aerosol acidity despite declining atmospheric sulfate concentrations over the past 15 years. Nat. Geosci. 9, 1–5. http://dx.doi.org/10.1038/NGEO2665.

Wiklund, J. a, Hall, R.I., Wolfe, B.B., Edwards, T.W.D., Farwell, A.J., Dixon, D.G., 2012. Has Alberta oil sands development increased far-field delivery of airborne contaminants to the Peace-Athabasca Delta? Sci. Total Environ. 433, 379–382. http://dx.doi.org/10.1016/j.scitotenv.2012.06.074.

Wyers, G.P., Otjes, R.P., Slanina, J., 1993. A continuous-flow denuder for the measurement of ambient concentrations and surface-exchange fluxes of ammonia. Atmos. Environ. Part A. Gen. Top. 27, 2085–2090. http://dx.doi.org/10.1016/0960-1686(93)90280-C.

Yu, X., Lee, T., Ayres, B., Kreidenweis, S., Malm, W., Collett, J.L., 2006. Loss of fine particle ammonium from denuded nylon filters. Atmos. Environ. 40, 4797–4807. http://dx.doi.org/10.1016/j.atmosenv.2006.03.061.

Yu, X., Lee, T., Ayres, B., Kreidenweis, S.M., Collett, J.L., Malm, W., 2005. Particulate nitrate measurement using nylon filters. J. Air Waste Manag. Assoc. 55, 1100–1110.

Zhou, Y., Shively, D., Mao, H., Russo, R.S., Pape, B., Mower, R.N., Talbot, R., Sive, B.C., 2010. Air toxic emissions from snowmobiles in yellowstone national park. Environ. Sci. Technol. 44, 222–228. http://dx.doi.org/10.1021/es9018578.